Article

Deuterium- and Alkyne-Based Bioorthogonal Raman Probes for In Situ Quantitative Metabolic Imaging of Lipids within Plants

Simon Sau Yin Law, Masato Asanuma, Jingwen Shou, Yasuyuki Ozeki, Yutaka Kodama, and Keiji Numata*
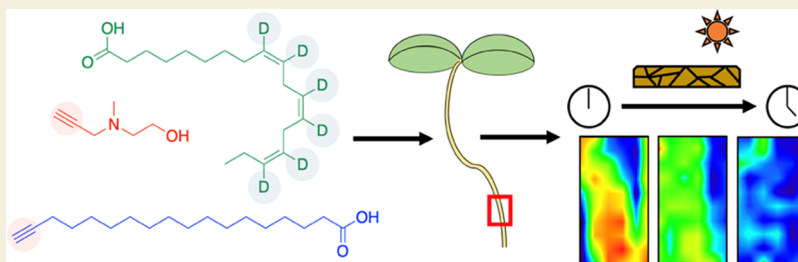
Cite This: *JACS Au* 2023, 3, 1604−1614

Read Online

ACCESS | Metrics & More | Article Recommendations | Supporting Information

ABSTRACT: Plants can rapidly respond to different stresses by activating multiple signaling and defense pathways. The ability to directly visualize and quantify these pathways in real time using bioorthogonal probes would have practical applications, including characterizing plant responses to both abiotic and biotic stress. Fluorescence-based labels are widely used for tagging of small biomolecules but are relatively bulky and with potential effects on their endogenous localization and metabolism. This work describes the use of deuterium- and alkyne-derived fatty acid Raman probes to visualize and track the real-time response of plants to abiotic stress within the roots. Relative quantification of the respective signals could be used to track their localization and overall real-time responses in their fatty acid pools due to drought and heat stress without labor-intensive isolation procedures. Their overall usability and low toxicity suggest that Raman probes have great untapped potential in the field of plant bioengineering.

KEYWORDS: *Raman spectroscopy, molecular probes, bioorthogonal probes, biosensors, stimulated Raman spectroscopy*

INTRODUCTION

Bioorthogonal molecular probes have been gaining tremendous research interest due to their potential applications in labeling and imaging molecules within biological systems in their native conditions.[1−3] Conventional fluorescence-based bioorthogonal probes usually contain conjugated fluorescence labels or a modified biological substrate conjugated with a chemical reporter, which can undergo a highly specific reaction with its reaction partner and thus be labeled and imaged by fluorescence microscopy.[3−7] For example, alkyne-containing probes can be conjugated through click chemistry with fluorescently tagged azide to label specific molecules that are introduced within cells.[3] This method has relatively high specificity but is difficult to adapt to dynamic real-time studies due to its nonreversible nature and relatively long labeling times. Furthermore, the inclusion of relatively bulky fluorogenic tags has also been shown to affect their intracellular distribution and metabolism.[8,9] Recently, a solvatochromic fluorescent probe was synthesized, could shift its emission wavelength based on the surrounding chemical environment, and could be metabolized through endogenous processes within hepatocytes, suggesting that further developments in bioorthogonal probes could have potential for metabolite imaging.[10]

Mass spectrometry (MS) imaging techniques have also been developed and utilized for in situ metabolite analysis that can be performed under ambient conditions.[11−13] Notably, matrix-assisted laser/desorption ionization and desorption electrospray ionization are commonly employed for MS imaging due to their rapid analysis, high sensitivity, and lateral resolution.[12,13] Infrared laser ablation has also seen use in plants due to its ability for spot-to-spot sampling with matrix-free measurements that allow for ionization and desorption of analytes directly from the sample surface.[13,14] Due to the accuracy and speed of MS measurements, a range of compounds can be detected unambiguously and simultaneously within a large spatial range.[15,16] However, challenges including the limited resolution due to the laser spot size (average ∼20 μm), sample damage, and limited penetration beneath the epidermal layer have hampered widespread adoption of MS for intracellular metabolite tracking

within plants. Despite these limitations, the use of MS imaging has been used to quantify a variety of metabolites within different plant tissues including sugars, lipids, and secondary metabolites, and considerable research efforts have been made to further develop general application of MS for single-cell resolution imaging.[16−20]

Renewed interest has also been placed on Raman-based probes, as they can be used for direct multiplex imaging of different biomolecules by tuning the attached chemical moiety in an endogenous environment. For applications within plants, an alkyne-tagged sucrose was recently developed as a method that could visualize sugar trafficking in real time within plant cells via sucrose transporters.[2] Deuterium (d) and alkynes have unique Raman signals in the cell-silent region (1900−2400 cm^{-1}) that are readily distinguished from endogenous species and can also be applied for quantification studies.[1,21−23] Furthermore, deuterium-labeled molecules have shown tremendous promise for use as Raman probes to image lipid droplets and detect pH changes within cells.[24−26] Despite decreased sensitivities compared with fluorescence-based probes, the flexibility of Raman tags has been used as intracellular probes to dynamically image molecules ranging from nucleic acids to phospholipids in a variety of cell types including animal cells.[27−31] However, even though there has been extensive development in imaging using biorthogonal Raman probes within animal cell-based studies, the application of molecular probes for metabolite studies within intact plants has remained relatively understudied and limited despite their potential applications in plant bioengineering and imaging. This may be due to differences between the different cell types as well as the strong intrinsic fluorescence of most plant cells that interferes with Raman spectroscopy.[2]

Lipids, such as those containing alkyl chains (fatty acids), as well as modified lipids, including glycerolipids and phospholipids, are important structural and signaling compounds within plant cells and their membranes.[32,33] Phospholipids are part of the lipid bilayers and play specific roles in development and function as signaling molecules.[34−36] In plants, phosphatidylcholine is among the most abundant phospholipids and plays an important role in abiotic stress response through the use of coordination of membrane signaling and trafficking processes.[36,37] It was previously demonstrated that proparagylcholine (PPG), an alkyne-containing choline analog, could be employed as a probe for choline phospholipids via a fluorescent azide click reaction and can be visualized within plants.[3] Saturated fatty acids in plants are mostly composed of triacylglycerols (TAGs), and their accumulation and metabolism have been proposed as a stress-adapting mechanism. Lipid droplets (LD), in which TAGs are stored, also function as subcellular compartments for substrates in the biosynthesis of useful plant compounds that elicit defense and stress responses.[38,39]

One of the most important families of alkyl fatty acids in plants is the C18 unsaturated fatty acids (UFAs), which encompasses oleates (C18:1), linoleates (C18:2), and α-linolenates (C18:3). These compounds are critical in the activation of stress response pathways, including the jasmonate, cutin/suberine, carbon/energy reserve, and membrane glycerolipid pathways.[38,40,41] Importantly, different UFAs (C12 to C20) can be rapidly interconverted through esterification or further modified into downstream bioactive molecules.[40] In tandem with the C18 UFAs, these derivatives are critical for regulating plant responses to biotic and abiotic stress by maintaining membrane fluidity and signaling pathways as well as stimulating oxygen production.[33,40] The plant stress response mechanisms that involve C18 UFAs and their derivatives are extremely versatile and allow for broad-spectrum defense from abiotic stresses within plants.[9,12]

In this study, we employ alkyne and deuterium-based Raman probes that mimic choline and C18 fatty acids to track and quantify uptake and metabolism within intact *Arabidopsis thaliana* (*A. thaliana*) roots and tobacco Bright Yellow-2 (BY-2) culture cells. The probes could be easily applied to the growth media during germination and were readily taken up by the plant cells without adverse effects and were localized analogously to their natural counterparts within the lipid droplets and the periphery within the roots. In addition, the probes exhibited detectable Raman signals within the intracellular UFA pools that followed overall intracellular distributions. Intracellular responses in unsaturated lipid levels to different abiotic stressors, such as heat and drought, could be monitored in real time by conventional Raman microscopy without the use of specialized equipment such as those used in stimulated Raman spectroscopy (SRS), increasing their potential in biosensor-based applications. The Raman results corroborated well with the quantification obtained by gas-phase chromatography−mass spectrometry (GC−MS). These results highlight the flexibility and ease of use of bioorthogonal Raman probes for real-time monitoring and quantification in plant systems and suggest that the probes can be applied to track other metabolic pathways as specific metabolites can be tagged within plants.

■ RESULTS AND DISCUSSION

Uptake and Localization of Bioorthogonal Raman Probes within Tobacco BY-2 Cells and *A. thaliana* Roots

We investigated the application of three bioorthogonal Raman probes for use within plants based on the roles they play in stress response pathways, including heat and drought stress (Figure S1). Two Raman probes containing alkyne moieties and one deuterium-labeled probe were investigated (Figure 1a) as potential metabolic probes within plants. Proparagylcholine (**1**; PPG) and 17-octadecynoic acid (**2**; 17-ODYA) were used as bioorthogonal probes of choline and octadecanoic acid with a modified alkyne terminal group, respectively (Figure 1a). Choline is a key component of phospholipid membranes and is readily incorporated into phosphatidylcholine and other membrane lipids through the Kennedy pathway.[36,42] Furthermore, PPG has been shown previously to function as a fluorescence-based click reaction probe for labeling cell membranes.[43] Octadecanoic acid in plants functions as both an energy storage in the fatty acid pool and is readily converted into other lipid species, including UFAs of different lengths.[44−47] The deuterated (C20-3) dihomo-γ-linolenic acid-d_6 (**3**; LA-d_6) was used as a bioorthogonal probe for assessing unsaturated fatty acid levels within *A. thaliana* in response to common abiotic stresses, due to the involvement of UFAs and its related metabolites in stress response pathways.[40,41,45]

We first measured each of the probes' Raman spectra in solution by dissolving the respective probe in ethanol (Figures 1 and S2). All three probes displayed the expected Raman signal in the cell-silent region (1900−2400 cm^{-1}), with a strong sharp peak at approx. 2130 and 2115 cm^{-1} for the alkynes (C≡C−H), which were detected within PPG and 17-ODYA, respectively (Figure 1b,c). The Raman signal for LA-d_6 was a significantly broader peak from 2100 to 2180 cm^{-1}, with less pronounced
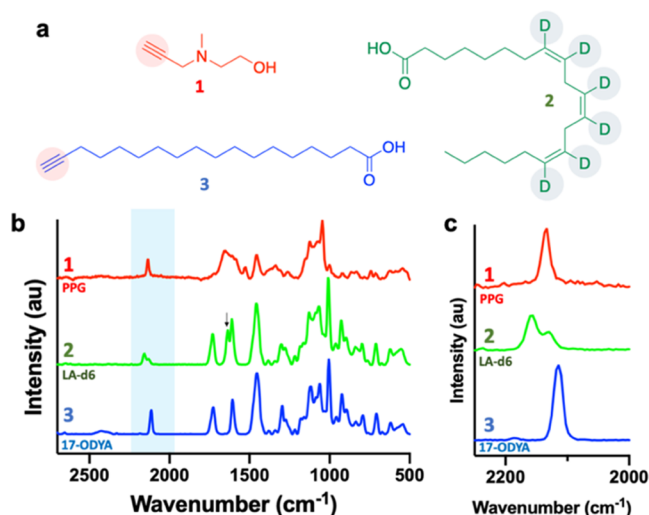
Figure 1. Raman spectra and chemical structure of the bioorthogonal probes. (a) Chemical structures of the (1) proparagylcholine (PPG), (2) dihomo-γ-linolenic acid-d_6 (LA-d_6), and (3) 17-octadecynoic acid (17-ODYA) probes used in this study. The alkyne and deuterium probes are highlighted in red and gray, respectively. (b, c) Raman solution spectra of the probes in (a) taken in solution (EtOH) and its inset (c) on the alkyne and deuterium region between 2000 and 2200 cm^{-1}. An additional D−C≡C−D peak can be seen at 1660 cm^{-1} for LA-d_6, as marked by the arrow (b).

peaks at 2130 and 2150 cm^{-1} from the C−D bands. An additional peak could be detected for LA-d_6 at 1640 cm^{-1} corresponding to D−C≡C−D stretching (Figure 1b), as indicated.

Next, we investigated whether the respective probes could be taken up within BY-2 model plant cells and detected intracellularly (Figure 2). Raman mapping of the respective signature Raman peaks for the labeled alkyne or deuterium in the cell-silent region (1900−2400 cm^{-1}) within the cell was performed after 3 h of incubation with the respective probes. For PPG, its distribution was found to be relatively uniform throughout the BY-2 cell, with higher concentrations within the vacuoles and the respective membranes found within the cell (Figure 2a), suggesting that it localized within the cell according to its expected endogenous distribution. Similar results were observed for the distribution of 17-ODYA within the cytosolic region of the cell, with almost no signal localized within the nucleus, which also matches well with previous results using other lipid-based probes within animal cells.[10,26] In contrast, the distribution of LA-d_6 was found mostly in the cytosol, with minimal signal observed within the vacuoles. The deuterium signal corresponding to LA-d_6 also significantly broadened, likely due to its low biomolecular specificity since it represents the sum of Raman signals from any C−D bond-containing metabolite derived from LA-d_6 that subsequently shifts the stretching band of the peak.[48]

We then examined the distribution of the three probes within *A. thaliana* by performing germination under normal growth conditions with reach respective probe spiked into the media during initial sowing. The Raman signals were detected in each of the three probes, particularly the root hairs of the plants (Figure 3). Uptake of PPG within the root cells of *A. thaliana* grown in the presence of probe (500 µM) was detected by the presence of the alkyne Raman peak at 2115 cm^{-1} (Figures 3a and S3) and reflected the distribution observed by fluorescent click chemistry previously reported.[3]

Interestingly, this distribution could be found most strongly within the center of the root, with decreasing concentrations toward the edges and relatively weak signals within the root hairs of the plants, unlike the other two probes. This distribution matches well with the actual physical profile of the main root when overlaid, suggesting that the probe distribution throughout the root was relatively uniform (Figure S3). We also confirmed the presence of PPG by staining it with fluorescently labeled TAMRA-azide, which labels free alkynes for confirmation by confocal laser scanning fluorescence microscopy
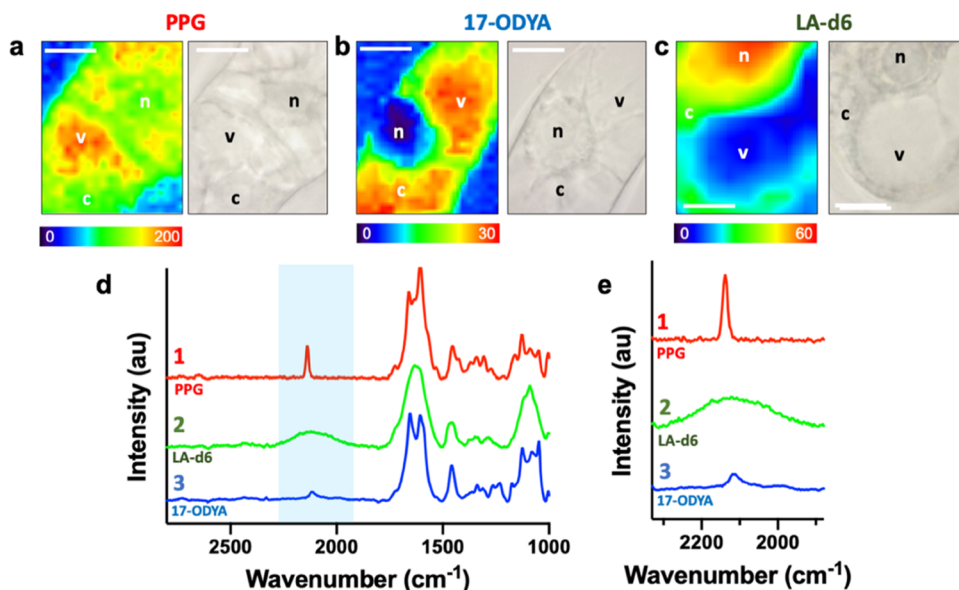
Figure 2. Raman probe localization in BY-2 cells. (a−c) Localization of (a) PPG, (b) 17-ODYA, and (c) LA-d_6 in BY-2 cells after 3 h of incubation with the respective probes. The scale bars represent 10 µm, and the color bars represent the unscaled Raman intensities for each representative image. Cellular components are labeled as nucleus (n), vacuole (v), and cytosol (c) in the bright-field images. (d, e) Averaged Raman spectra for the respective maps shown in (a−c) and its inset (e) on the alkyne and deuterium region between 2000 and 2200 cm^{-1}.
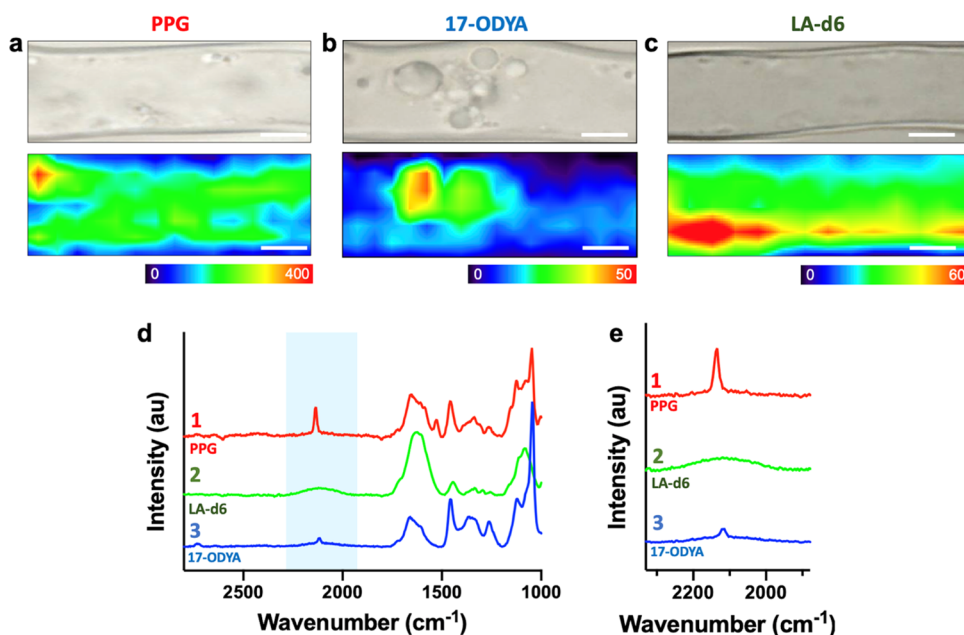
Figure 3. Raman probe localization in *A. thaliana* root hairs. (a−c) Localization of (a) PPG, (b) 17-ODYA, and (c) LA-d_6 in BY-2 cells grown from *A. thaliana* seeds in 1/2 MS plates containing the respective probes. The scale bars represent 5 μm, and the color bars represent the unscaled Raman intensities for each representative image. (d, e) Averaged Raman spectra for the respective maps shown in (a−c) and its inset (e) on the alkyne and deuterium region between 2000 and 2200 cm^{-1}.

(CLSM) (Figure S3).[3] Strong fluorescence could be observed within the roots that were similar to the Raman signal distribution, providing evidence that the observed Raman signals were from PPG within the plant (Figure S3).

Next, we investigated the uptake of the two fatty acid-based probes (17-ODYA and LA-d_6) within the root cell (Figure 3b,c). Interestingly, large lipid bodies were found within the root hair cells of the plants that were grown in the presence of 17-ODYA (Figure 3b) that could be seen to dynamically shift in real time (Video S1). These lipid bodies have been previously demonstrated to play important signaling roles in addition to storage for lipids, including dynamic transport of their contents with other intracellular destinations during signal transduction, and further suggests that these molecules could be used to probe such pathway mechanisms.[49,50]

We further confirmed the presence of these lipid droplets by staining them with the lipid stain Nile Red (Figure S4) and observed strong staining for both the probe-treated and control samples treated with unlabeled probes. These large lipid bodies were not found in plants grown without the added probe, suggesting that the formation of these lipids was induced by the addition of the FA in the media and that the probe could elicit the same response as that of the unlabeled counterpart (Figure S4). Increased alkyl signals could also be observed in the lipid droplet locations and suggest overall increases in fatty acids (Figure S4).

In *A. thaliana* incubated with LA-d_6, a broadened Raman signal was observed, which was similar to that in BY-2 cells, and stronger signals were localized near the interior of the root (Figure 3c). However, there was considerably less signal variation within the root, with concentration near the lipid droplets at the periphery of the root. Overall, the Raman results from BY-2 and *A. thaliana* suggest that all three labeled probes are able to localize within the respective cells analogously to their endogenous counterparts.[3]

## Effect of Drought Stress on Linolenic Acid Metabolism within *A. thaliana*

Due to the role that UFAs play in stress responses, including responses to drought and heat, we next investigated the application of LA-d_6 and 17-ODYA to monitor their real-time changes in plants upon abiotic stress. In particular, we focused on UFAs and their derivatives since they are directly regulated within the drought stress response by altered lipid compositions and fatty acid metabolism.[37,39,41]

For a constant drought stress due to water deficit, we simulated low water potential using PEG-infused plates with a water deficit of −0.7 MPa.[51] Seeds of *A. thaliana* were germinated in the presence of LA-d_6 until the seedlings size reached 4 cm (7 days old), were transferred to PEG-infused plates to induce a drought response (1 to 2 days), and were recovered in H$_2$O in situ during Raman microscopy (Figure S5). We first examined the effect of drought and subsequent recovery in water by measuring the deuterium Raman peak using stimulated Raman scattering (SRS) to map the broad deuterium peak previously identified (2080 cm^{-1}).

We observed similar distributions to the previous Raman microscopy results after drought treatment, with a strong localized signal on the boundary of the root cell (Figure 4a). However, upon water recovery, this signal slowly attenuated (Figure 4a); the signal intensity was approximately halved after 30 min and diminished to 30% of the original intensity at 60 min. This suggests that a strong response to the LA-d_6 signal occurs after drought and subsequent water recovery. In addition, the results reflect previous studies that investigated UFAs lipidomes and their diverse roles in plants for drought stress responses, including glycerolipids, oxylipin biosynthesis, stress signaling and reserves of energy.[40,52] The response to drought stress and subsequent water recovery suggests the potential for LA-d_6 to function as a probe for tracking its intra- and intercellular dynamics.
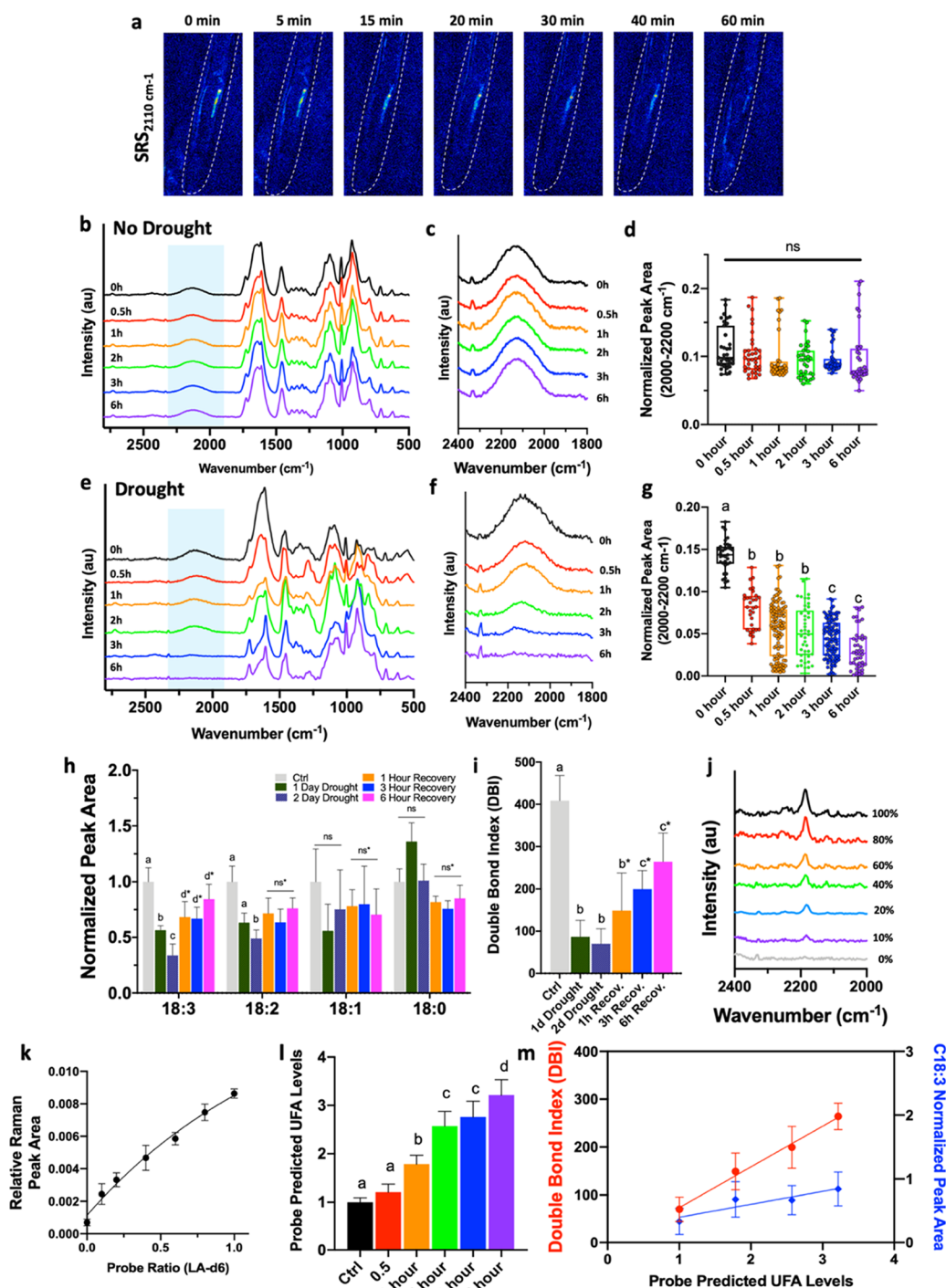
Figure 4. Spatiotemporal metabolic imaging and quantification of linolenic acid and C18 fatty acids using LA-d_6 in *A. thaliana* roots under drought stress and water recovery. (a) Real-time SRS imaging at 2110 cm^{-1} of LA-d_6 localization in 1-week-old *A. thaliana* postdrought treatment (2 days) and recovered in water (min). The dotted line highlights the root hair boundary. The width of each image is 25 μm. (b, c) Average spectra from confocal Raman mapping of *A. thaliana* seedlings incubated with LA-d_6 without drought treatment and subsequent incubation in H_2O and its inset (c) showing the Raman region between 1900 and 2200 cm^{-1}. (d) Normalized peak areas for the 2000−2200 cm^{-1} region for individual spectra taken from confocal Raman mapping. (e, f) Average spectra from confocal Raman mapping of *A. thaliana* seedlings incubated with LA-d_6 with drought treatment for 1 and 2 days and subsequent recovery in dH_2O and the inset (f) showing the Raman region between 1900 and 2200 cm^{-1}. (g) Normalized peak areas for the 2000−2200 cm^{-1} for individual spectra taken from confocal Raman mapping. (h) Normalized peak area for C18 fatty acids as measured by GC−MS from fatty acids isolated from seedlings after drought and subsequent recovery. (i) Double bond index analysis to estimate the degree of unsaturation in the lipids calculated by the abundance from (h). DBI = 1 × % monosaturated fatty acids + 2 × % diunsaturated fatty acids + 3 × % triunsaturated fatty acids. (j) Deuterium peak areas from LA-d_6 in a matrix of palmitic acid/plant lysate with varying probe solution ratios. (k) Relative Raman peak area from (i) plotted against the relative probe ratio. (l) Relative unsaturation levels estimated from normalized peak areas in (g) relative to the peak heights observed at 0 h recovery. (m) Linear relationship observed between relative unsaturation levels measured by Raman microscopy in (l) with DBI (i) and C18:3 quantification (f) as determined by GC−MS.
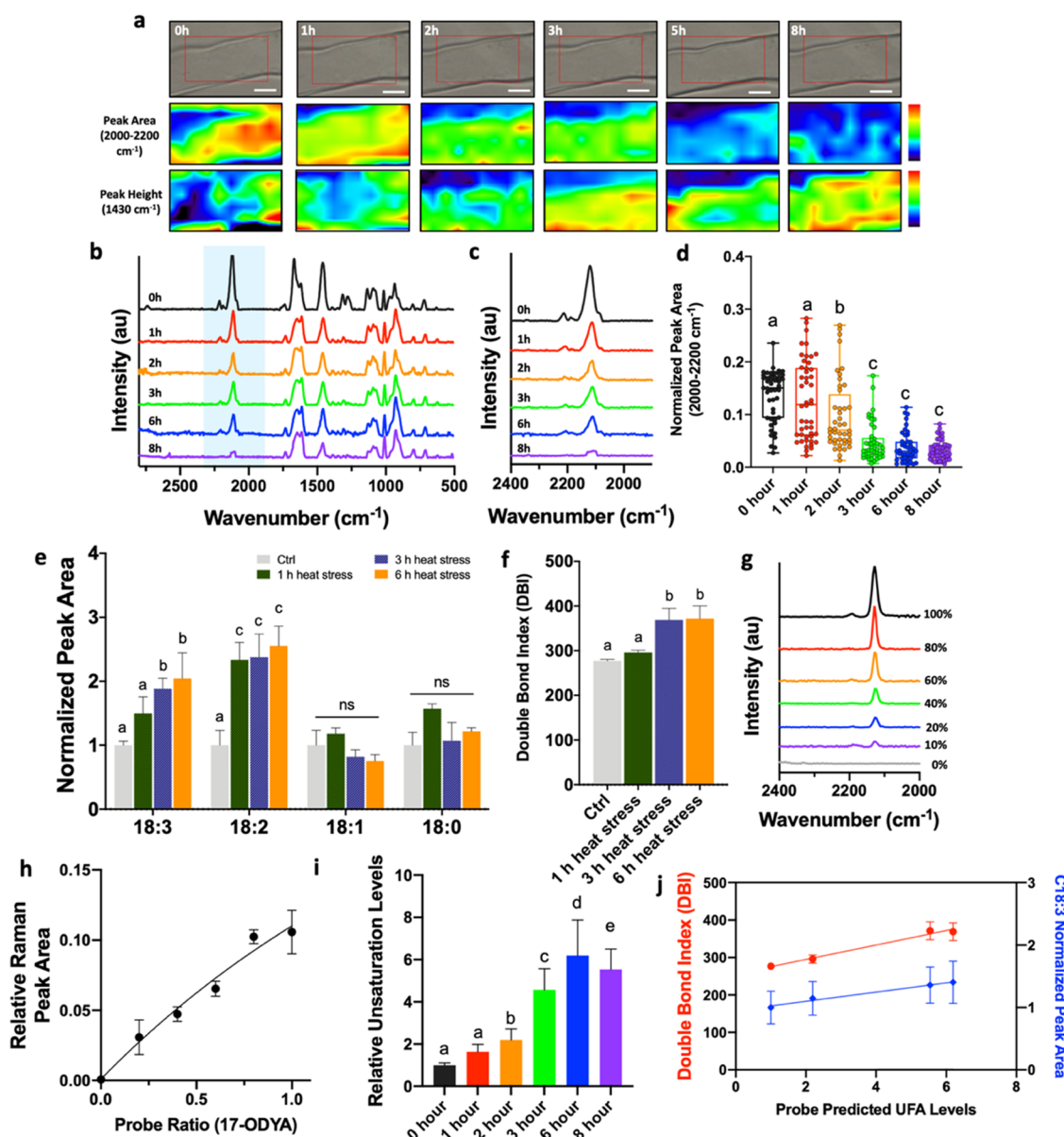
Figure 5. Spatiotemporal metabolic imaging of C18 fatty acids and quantification using 17-ODYA in *A. thaliana* roots under heat stress. (a) In situ confocal Raman mapping of *A. thaliana* seedlings under heat stress at 35 °C from 0 to 8 h showing the relative intensity of the alkyne peak from 17-ODYA at 2120 cm^{-1}. The confocal light image (top), the relative alkyne peak areas at approx. 2000−2200 cm^{-1} (middle), and the peak height at 1430 cm^{-1} corresponding to C−H stretching as a control for the overall fatty acid content. The scale bars represent 2.5 μm, and the color bars represent the scaled Raman intensities for each representative image for the respective time course. (b, c) Average spectra from confocal Raman mapping of *A. thaliana* seedlings grown with 17-ODYA under heat stress at 35 °C from 0 to 8 h and its inset (c) at 1900−2400 cm^{-1}. (d) Normalized peak areas for 2000−2200 cm^{-1} for individual spectra taken from confocal Raman mapping (min. $n = 30$). (e) Quantification of normalized peak area for 18C fatty acids as measured by GC−MS from fatty acids isolated from seedlings before and after heat stress. (f) DBI analysis to estimate the degree of unsaturation in C16 and C18 lipids calculated from (e) DBI = 1 × % monounsaturated fatty acids + 2 × % diunsaturated fatty acids + 3 × % triunsaturated fatty acids. (g) Alkyne peak areas from 17-ODYA in a matrix of 2% stearic acid/plant lysate solution with varying probe-to-matrix ratios. (h) Relative Raman peak area from (g) plotted against the relative probe ratio. (i) Relative unsaturation levels estimated from the normalized peak areas in (d) relative to the peak heights observed at 0 h recovery. (j) Linear relationship observed between DBI and C18:3 unsaturated fatty acid levels and the corresponding probe signal observed in the 17-ODYA Raman signal.

To quantify the deuterium peak in the spectra, we imaged the root cells using conventional Raman microscopy and performed GC−MS at 0 days (control), 1 day, and 2 days after drought stress and subsequent recovery in water for up to 6 hours (Figure 4b−h). Growth was significantly inhibited by the drought treatment compared with the control samples (Figure S6), with a significant decrease in root growth relative to the control samples grown in normal media. Quantification of the root areas

showed a 20% decrease on average in relative root areas during the first 2 days (Figure S6).

Subsequent quantitative analysis of the root hairs and overall lipid unsaturation levels was performed using conventional Raman microscopy mapping of the root hairs. For the overall quantification of probe levels and lipid unsaturation, average spectra are shown for the mapped area (40 by 20 μm) (Figure 4b−e). We observed the same strong deuterium signals (2000−

2200 cm^{-1}) within the cell membrane as the respective root cells observed in the previous experiments in both the untreated (Figure 4b,c) and drought-treated samples (Figure 4e,f). For the untreated samples (Figure 4b−d), the deuterium signal remained stable throughout (the quantification is shown in Figure 4d), suggesting that probe levels were relatively stable. However, for the *A. thaliana* samples that were subjected to drought, we observed a similar reduction in the Raman signal observed with SRS (Figure 4a) in response to water recovery (Figure 4e,f). Quantification of the observed peak further confirmed this reduction and showed an approximately 50% reduction in the signal after 1.5 h of recovery and an 80% reduction after 4 h of recovery (Figure 4g).

Next, by GC−MS, we further confirmed these results by analyzing the fatty acids extracted from homogenized *A. thaliana* seedlings after 1 or 2 days of drought treatment and subsequent water recovery conditions (1, 3, 6 h) (Figure 4h). At both one and two days of drought treatment, a significant decrease in most of the UFAs (C18:3, C18:2, C18:1, C16:3, and C16:2) was observed, agreeing with previous research in that the overall levels of unsaturation of intracellular lipids decrease upon drought stress in plants (Figures 4h and S7).[33,40]

However, upon recovery in water, lipid unsaturation quickly increased and was approx. 15% less than that of untreated samples after 6 h of treatment for C18:3. To quantify the overall unsaturation levels of the C16 and C18 lipids, the double bond index (DBI) was used to quantify the relative amount of unsaturated lipids in each sample before and after treatment and subsequent recovery (Figure 4i). The DBI significantly decreased from approx. 400 to 65% upon drought treatment after 2 days, and subsequent recovery was observed in the individual lipids as soon as 1 h of incubation within water and reached 60% of the predrought levels after 6 h of recovery in water (Figure 4i).

Since LA-d_6 could be internalized and distributed analogously within the root hairs in the plants as a major C18:3 FA that could be interconverted to other UFA species, we investigated whether the detected Raman signal could be used as a predictor of intracellular UFA levels.[53] We first examined the signal response of LA-d_6 in a plant cell lysate/2% stearic acid solution (Figure 4j,k) by varying the probe concentration from 0 to 100%. A direct concentration dependence in the Raman signal peak area could be observed in both the averaged spectra (Figure 4j) and the quantified peak areas (Figure 4k), suggesting that the overall changes within the peak area could be used to quantify the relative probe concentration from the Raman spectra.

For semiquantitative analysis of intracellular LA-d_6 (Figure 4l), we measured the proportional peak area for the individual measured Raman spectra relative to the peak areas observed immediately after drought (0 h recovery), as shown in Figure 4d. Due to the rapid decrease in Raman signal observed and the rapid recovery of the DBI after recovery within water upon drought treatment, we speculated that it was possible to detect overall unsaturation levels of lipids found in the plants by using LA-d_6 as a probe. When LA-d_6 is taken up intracellularly, its concentration likely remains relatively constant over the measured time periods, as noted by the non-drought control (Figure 4b−d). However, as the equilibrium in the synthesis and liberation of unsaturated lipids causes the overall concentration of the probe to decrease relative to the overall fatty acid level, the overall intracellular concentration of the probe rapidly decreases.

This is also supported by previous studies investigating that LA-related genes were shown to elicit the plant's defense mechanisms through upregulation of galactinol synthase enzymes during abiotic stress including drought.[53] Furthermore, the downstream metabolites of the LA pathways including the jasmonates have also been demonstrated to be mobilized during abiotic stress as precursors for numerous aliphatic compounds in the plant defense response and rapidly respond to drought withdrawal, supporting the rapid decrease in Raman signal that we observed in Figure 4f upon removal from drought stress.[52,54]

By plotting the Raman-predicted UFA levels with those determined from GC−MS and overall DBIs, we observed a strong linear correlation between the Raman-predicted ratios and those obtained by GC−MS (Figure 4l,m). The decrease in the Raman probe calculated ratios mirrored the decrease in DBI and levels of the C18:3-C18:1 UFA levels (Figure 4m); this result suggests that our probe functions bioorthogonally and can be used to predict overall lipid unsaturation levels within the roots of *A. thaliana* in response to drought stress. However, there is an outsized effect in the reduction of the probe compared to the DBI or UFA levels determined by GC−MS. We surmise that this is because mobilization of the labeled LA-d_6 likely occurs in the stress response pathways as well as an overall transport of fatty acids away from the root hairs as recovery occurs. Nonetheless, the Raman signal from the probe tracked both overall unsaturation levels and C16 and C18 UFAs.

Effect of Heat Stress on Fatty Acid Distribution and Concentration within *A. thaliana*

Due to the roles of UFAs in cell metabolism and the heat stress response, we next investigated the use of 17-ODYA as a way to monitor the heat stress response in UFAs as a defense mechanism for overall lipid metabolism and localization within the roots. Previous studies have shown that heat stress stimulates a general increase in TAG markers within plants due to general stress response pathways upregulated by heat.[39,41,53] General upregulation of acyltransferases induces TAG accumulation outside of chloroplasts in plants subjected to heat stress, and their subsequent accumulation within both the shoots and roots.[53,55]

We subjected 1-week-old seedlings grown in the presence of 17-ODYA to heat stress (35 °C) in situ via a heated sample chamber during Raman microscopy (Figure S5). We determined the localization of 17-ODYA in three distinct roots by performing Raman mapping (30 μm × 16 μm) (Figure 5a), in which a total of 45 spectra were collected per time point, to measure the specific alkyne signal with normalization to the general alkyl region (Figure 5b,c). Overall, the alkyne signal was attenuated significantly over time under heat stress from 2 h until 6 h (Figure 5b,c). This was reflected in both the mapping and the average Raman spectra, in which the quantified alkyne peak areas (Figure 5d) sharply decreased by 75% after 4 h of heat stress.

Similar to the drought stress experiments, we next quantified the isolated UFAs by GC−MS (Figures 5e, S8, and S9). General unsaturated lipids for both C18 and C16 were elevated as expected for plants under heat stress, with C18:3 and C18:2 having an observed 100% increase in relative peak areas one to 6 h after heat stress was applied. General unsaturation levels within the plants were estimated using the DBI index (Figure 5f) and reflected the results observed in GC−MS with a significant increase in DBI at 3 and 6 h of heat stress.

The overall fold-changes in UFA concentrations were then estimated from the attenuation of the Raman signal over time from heat stress. Since the probe levels also followed a similar trend during water recovery after drought stress, we next looked at the probe response to heat stress to see if it could be used as a predictor of UFA levels within the plants upon heat stress. We confirmed the response of the probe in a similar fashion as before with a plant lysate/2% stearic acid solution and varying the probe concentration from 0 to 100%. A concentration-dependent decrease in the Raman signal was observed in both the spectra and quantified peak areas (Figure 5g,h), suggesting that the concentration response of 17-ODYA was similar to that observed for LA-d_6 (Figure 4j,k).

Due to the increase in overall fatty acid species after heat stress, which was similar to those observed in the drought stress experiments, we predicted that the changes in lipid distribution determined from GC−MS would also be reflected in the observed decrease in Raman signal as 17-ODYA enters the intracellular fatty acid pool. We quantified the alkyne peak area corresponding to the probe by comparing it with the control peak area (0 h) before heat stress was applied (Figure 5i). As the ratio of the label to the total pool of FA decreases, a subsequent decrease in the overall alkyne signal is observed. This is also reflective of the total UFA pool within the plant as it changes its FA composition in response to the stress compared with the DBI and C18:3 and C18:2 levels (Figure 5j). The linear correlation between the overall DBI and C18:3 levels and the Raman signal from the probe (Figure 5j) suggests that similar to LA-d_6, 17-ODYA could also detect overall changes in the FA pools within the plants in response to heat stress. We note that, similar to the drought stress response, the UFA-fold changes predicted by the probe peak were exaggerated, and we predicted that this was likely because 17-ODYA itself was also likely metabolized or liberated from the roots, causing an outsized effect on the decrease in signal intensity with regard to the probe. These results demonstrate that 17-ODYA within the root responded dynamically to heat stress and could be metabolized similarly to its endogenous counterpart, which could be quantified in real time using Raman microscopy. Significant increases in C18:3 and C18:2 levels were observed upon heat stress and matched well with previous studies that examined fatty acid levels within plants under heat stress, further supporting the responses in probe signal reflecting intracellular metabolite changes.[39,41]

Taken together with the drought stress data, these results suggest that both LA-d_6 and 17-ODYA can be readily taken up into plants by simple addition into the growth media and subsequently detected intracellularly by conventional Raman spectroscopy. Despite the slight thermal damage induced by long measurement times by Raman microscopy, quantification of the overall Raman signals remained consistent throughout for the three tested probes and suggests that they are able to function in the tested time frames (Figure 4b). Their distributions also mimicked their unlabeled counterparts, and in the case of 17-ODYA, induced the formation of lipid bodies similar to unlabeled stearic acid (Figure S3). Quantification of their respective Raman signals also correlated well with GC−MS quantification, suggesting potential for further development in studies on distinct cellular pathways by introducing specific labeled metabolites in a similar fashion. Furthermore, due to their responses to stress factors that mirror their endogenous counterparts, these Raman probes can be used as a highly flexible and noninvasive method for monitoring intracellular UFA levels within plants.

CONCLUSIONS

Performing in situ monitoring of individual metabolites has historically been challenging due to the complicated endogenous cellular milieu with high concentrations of complex compounds.[10,25,56] This is further complicated by the differences between plant and animal cells since most probes developed for animal cells cannot be immediately applied for plant-based studies. General imaging techniques such as mass spectrometry imaging have been used to overcome these limitations within metabolite research for biomedical applications due to their high sensitivity and multiplex capabilities.[11,13] Despite limitations in spatial resolution and tissue damage, they have shown tremendous promise for fast and direct imaging of intracellular molecules without the development of specific probes.[16]

Conversely, bulky bioorthogonal probes, such as those with fluorescent tags or click chemistry reactivities, represent highly specific probes with strong potential for multiplex imaging applications. However, large tags often interfere with their endogenous metabolism and localization and potentially their cellular dynamics, hampering their applications in studying metabolic processes.[1,57] The small Raman molecular probes, such as deuterium- and alkyne-labeled fatty acids, that were employed in this study have shown promise in overcoming these shortcomings and have demonstrated application for metabolite imaging. These fatty acids have significant roles in maintaining plant health and responses to external stress and chemical tools to study their distribution and quantification of changes would allow for their characterization in a variety of bioengineering applications.

In summary, the Raman probes developed in this study represent a significant step forward in metabolite imaging and quantification within plants. The respective fatty acid probes are able to localize within intact *A. thaliana* and can be detected by conventional Raman spectroscopy for both quantification and localization without the use of time- and labor-consuming isolation steps. They can function in a bioorthogonal manner and are able to respond within endogenous UFA pools according to abiotic stress response pathways for heat and drought. Quantification of the probe response can enable real-time monitoring and tracking of precise UFA distributions for the dynamic studies of stress responses in bioengineering and intracellular molecular sensor applications without SRS imaging. Furthermore, this strategy can likely be expanded to study other metabolites and conditions, including abiotic stress or pathogen monitoring, for which current molecular toolkits are lacking.

EXPERIMENTAL SECTION

Materials

PPG (#25870: Batch 0542165-4), 17-ODYA (#90270; Batch 0 475470-39), and LA-d_6 (#10458; Batch 0560066-2) were purchased from Cayman Chemicals Ltd. 0.5× Murashige and Skoog (MS) (M5519) and other media components including PEG-8000 were purchased from Sigma-Aldrich. All probes are certified to be ≥99% as per the individual batch ID. Detailed certificates of analysis including MS and NMR are also available. BY-2 cells were obtained from the RIKEN BRC Experimental Plant Division.

BY-2 Cell and *A. thaliana* Growth Conditions for Incorporating the Probe

Seeds of *A. thaliana* Col-0 were germinated on 1/2× Murashige and Skoog (MS) media plates containing 2.5 mM MES, 1% sucrose, and 0.3% (w/v) agarose under 16/8 h light/dark periods at 22 °C for *A. thaliana*. Seven-day-old seedlings were used for experiments unless

otherwise noted. The BY-2 cells were grown in Murashige-Skoog (MS) medium supplemented with 3% (w/v) sucrose, 0.2 g L^{-1} KH_2PO_4, 1 mg L^{-1} thiamine-HCl, 0.1 g L^{-1} myo-inositol, and 0.2 mg L^{-1} 2,4-dichlorophenoxyacetic acid (2,4-D) (adjusted to pH 5.8). The cultures were stored in the dark at 26 °C and subcultured once per week. Log phase cells (3 or 4 days after culture) were used throughout the study unless otherwise stated. Delivery of each respective probe was achieved by incorporation into the media (200 μM for each respective probe), in which the seeds were germinated when the seeds were sown. For BY-2 cells, the probes were incubated with the culture for 3 h before measurement with excess probe, which was removed by centrifugating the cells at 100 × g for 5 min, and the cells were washed with 1/2 MS media three times before Raman measurements.

A. thaliana Growth Conditions and Respective Drought/Heat Stress Conditions

A. thaliana Col-0 seeds were germinated on 1/2MS (Sigma-Aldrich) medium plates under 16-/8-h light/dark periods at 22 °C for A. thaliana. Samples containing the respective probes were added just prior to seed germination. Drought conditions were prepared by adding 10 mL of PEG-8000 solution from the 1/2 MS plates that was poured off after 24 h. A. thaliana seedlings were then moved from the normal plates onto the PEG-infused plates for drought stress studies. Control samples were moved to a separate 1/2MS plate without a probe. The incubation conditions for drought treatment were otherwise unchanged from the initial germination conditions. Recovery in water was performed in situ on the microscope slide during Raman analysis. Heat stress was performed using a heated sample chamber incubated at 35 °C directly as the individual seedlings were measured by Raman microscopy.

Confocal Raman Microscopy Analysis

Confocal Raman microscopy analysis was performed using a JASCO NRS-4500 Raman Microscope (JASCO, Japan). Raman spectra taken on BY-2 cells or A. thaliana seedling samples at 63× magnification were performed on a microscope slide (SUPERFROST WHITE, S2441, Japan) with a cover glass using a 50 mW green laser at 532 nm (UPLSAPO 100XO, Olympus, Japan) and a slit size of 100 μm × 8000 μm. Raman mapping was performed using 2 μm steps with dimensions outlined in the respective image with collection times of 5 s at 25% intensity. Raman spectra of probes or probe/lysate samples were taken directly using a cover glass on a microscope slide with collection times of 1 s and a laser intensity of 100%.

All spectra were initially processed identically with default cosmic ray and fluorescence background removal. For qualitative comparisons between samples, spectra were normalized to their respective total area. For quantitative analysis, the spectra were averaged for the entire measured area shown in each figure of the respective probe to obtain a representative spectrum for each sample and were graphed accordingly. Peak areas were then used to generate the mapped intensity within the mapping image found in Figures 2−5. The peak areas were normalized to the alkyl peak at 2800−3000 cm^{-1} to normalize for differences between spectra unless otherwise noted. Average spectra used in Figures 2−5 were calculated over the entire imaged area as a numerical average of all data points collected in each mapped dataset.

SRS Raman Microscopy Analysis

SRS samples were prepared similarly to the Raman microscopy samples and were visualized at 60× magnification and a numerical aperture of 1.2 using a homemade SRS microscope.[29,31,58] Briefly, picosecond pump pulses at a wavelength of 843 nm were generated by a Ti:sapphire laser, and wavelength-tunable Stokes pulses at ~1030 nm were generated by an in-house built Yb fiber laser synchronized to the pump laser. The pump and Stokes pulses were combined with a dichroic mirror and sent to a laser scanning SRS microscope, where they were focused by a water immersion objective lens (60´, NA = 1.2). The sample was held in place with two coverslips. The optical power of the pump and Stokes pulses was estimated at the sample plane to be ~75 and ~55 mW, respectively. The transmitted pump pulses were detected by a photodiode, and its output was sent to a lock-in amplifier to obtain the SRS signal.

Spectra were measured in a 300 cm^{-1} window (1900−2200 cm^{-1}), and the SRS data were acquired with LabVIEW-FPGA software. The SRS data were processed using MATLAB to generate the SRS spectra, and ImageJ to generate cell images (500 × 500 pixels). Subsequent quantification was taken as the difference in heights between 1950 cm^{-1} and the peak of the signal at 2110 cm^{-1}. Respective signal heights were then mapped, and images were generated for each time point in situ during measurements in water using ImageJ Fiji (Version 2.1.0).

GC−MS Analysis of Extracted Lipids

The procedure for lipid extraction was based on a modified protocol previously described for UFAs and lipid derivative isolation from intact plants.[59,60] Briefly, 6−8 A. thaliana seedlings were frozen in liquid N_2 and ground to a fine powder using a mortar and pestle. Lipids were extracted with 1 mL citric acid (50 mM) in H_2O/acetone (30/70%) and sonicated for 20 min at RT. The samples were then centrifuged at 13,000g, and the acetone was evaporated with a constant N_2 stream. The citric acid phase was then extracted twice with diethyl ether (500 μL) and combined in another vial. The ether was then removed completely under a N_2 stream. Methanolysis was performed by adding 100 μL of a 15% HCl/methanol solution (v/v) and incubating the solution at 30 °C overnight. The acid was neutralized with an equivalent volume of 1 M NaCl and extracted twice with 200 μL hexanes. The combined hexane fractions were then evaporated to dryness with a stream of N_2 and resuspended in 80 μL of hexanes before GC−MS analysis.[61] UFAs were analyzed using a chromatography−mass spectrometry (GC−MS) instrument (GCMS-QP2010 Ultra, Shimadzu, Kyoto, Japan) equipped with a 30 m × 0.25 mm × 0.25 μm DB-1 capillary gas chromatography column (Agilent Technologies, CA). The injection temperature was set at 250 °C with splitless injection, and the interface temperature was 230 °C. The column temperature program for fatty acid ester separation was adopted from previous research[61,62] as follows: 45 °C for 1 min, a temperature gradient of +15 °C per min to 250 °C. Helium was used as the carrier gas with a flow rate of 3.30 mL min^{-1}. The relative UFA content was normalized to the respective total peak areas in each chromatogram with an internal C18 standard.

Statistical Analysis

GraphPad Prism 8.0 (GraphPad) was used for statistical analysis. Samples were compared using one-way analysis of variance (ANOVA) and Kruskal−Wallis tests to analyze significant differences under different treatment conditions. Differences between two means were considered statistically significant at $P < 0.05$ and indicated with asterisks (*). Data in experiments are expressed as the mean ± standard deviation unless otherwise noted, and sample sizes are stated in each respective figure.

■ ASSOCIATED CONTENT

ⓢ Supporting Information

The Supporting Information is available free of charge at https://pubs.acs.org/doi/10.1021/jacsau.3c00041.

Schematic of Raman probes used in this study, confirmation of their localization within A. thaliana roots using fluorescent labels, effect of drought on root growth, and GC−MS quantification of C16 lipids (PDF)

Dynamic movement of lipid droplets within the root hairs of A. thaliana as visualized within Raman microscope (AVI)

■ AUTHOR INFORMATION

Corresponding Author

Keiji Numata — *Biomacromolecules Research Team, RIKEN Center for Sustainable Resource Science, Wako, Saitama 351-0198, Japan; Department of Material Chemistry, Kyoto University, Kyoto 615-8510, Japan;* ⓞ orcid.org/0000-0003-2199-7420; Email: numata.keiji.3n@kyoto-u.ac.jp

Authors

Simon Sau Yin Law − *Biomacromolecules Research Team, RIKEN Center for Sustainable Resource Science, Wako, Saitama 351-0198, Japan;* ◉ orcid.org/0000-0002-9650-2958

Masato Asanuma − *Graduate School of Engineering, University of Tokyo, Tokyo 113-8656, Japan*

Jingwen Shou − *Graduate School of Engineering, University of Tokyo, Tokyo 113-8656, Japan*

Yasuyuki Ozeki − *Graduate School of Engineering, University of Tokyo, Tokyo 113-8656, Japan;* ◉ orcid.org/0000-0002-9004-0799

Yutaka Kodama − *Biomacromolecules Research Team, RIKEN Center for Sustainable Resource Science, Wako, Saitama 351-0198, Japan; Center for Bioscience Research and Education, Utsunomiya University, Utsunomiya, Tochigi 321-8505, Japan;* ◉ orcid.org/0000-0002-4720-7311

Complete contact information is available at:
https://pubs.acs.org/10.1021/jacsau.3c00041

Notes

The authors declare no competing financial interest.

■ REFERENCES

(1) Wei, L.; Hu, F.; Shen, Y.; Chen, Z.; Yu, Y.; Lin, C.-C.; Wang, M. C.; Min, W. Live-Cell Imaging of Alkyne-Tagged Small Biomolecules by Stimulated Raman Scattering. *Nat. Methods* **2014**, *11*, 410−412.

(2) Moliner, F.; Knox, K.; Gordon, D.; Lee, M.; Tipping, W. J.; Geddis, A.; Reinders, A.; Ward, J. M.; Oparka, K.; Vendrell, M. A Palette of Minimally Tagged Sucrose Analogues for Real-Time Raman Imaging of Intracellular Plant Metabolism. *Angew. Chem., Int. Ed.* **2021**, *60*, 7637−7642.

(3) Paper, J. M.; Mukherjee, T.; Schrick, K. Bioorthogonal Click Chemistry for Fluorescence Imaging of Choline Phospholipids in Plants. *Plant Methods* **2018**, *14*, No. 31.

(4) Dou, Y.; Wang, Y.; Duan, Y.; Liu, B.; Hu, Q.; Shen, W.; Sun, H.; Zhu, Q. Color-Tunable Light-up Bioorthogonal Probes for In Vivo Two-Photon Fluorescence Imaging. *Chem. - Eur. J.* **2020**, *26*, 4576−4582.

(5) Lo, K. K.-W. Molecular Design of Bioorthogonal Probes and Imaging Reagents Derived from Photofunctional Transition Metal Complexes. *Acc. Chem. Res.* **2020**, *53*, 32−44.

(6) Simon, C.; Lion, C.; Spriet, C.; Baldacci-Cresp, F.; Hawkins, S.; Biot, C. One, Two, Three: A Bioorthogonal Triple Labelling Strategy for Studying the Dynamics of Plant Cell Wall Formation In Vivo. *Angew. Chem., Int. Ed.* **2018**, *57*, 16665−16671.

(7) Sunwoo, K.; Bobba, K. N.; Lim, J.-Y.; Park, T.; Podder, A.; Heo, J. S.; Lee, S. G.; Bhuniya, S.; Kim, J. S. A Bioorthogonal 'Turn-on' Fluorescent Probe for Tracking Mitochondrial Nitroxyl Formation. *Chem. Commun.* **2017**, *53*, 1723−1726.

(8) Jensen, E. C. Use of Fluorescent Probes: Their Effect on Cell Biology and Limitations. *Anat. Rec.* **2012**, *295*, 2031−2036.

(9) Lavis, L. D.; Raines, R. T. Bright Building Blocks for Chemical Biology. *ACS Chem. Biol.* **2014**, *9*, 855−866.

(10) Kajiwara, K.; Osaki, H.; Greßies, S.; Kuwata, K.; Kim, J. H.; Gensch, T.; Sato, Y.; Glorius, F.; Yamaguchi, S.; Taki, M. A Negative-Solvatochromic Fluorescent Probe for Visualizing Intracellular Distributions of Fatty Acid Metabolites. *Nat. Commun.* **2022**, *13*, No. 2533.

(11) Wu, C.; Dill, A. L.; Eberlin, L. S.; Cooks, R. G.; Ifa, D. R. Mass Spectrometry Imaging under Ambient Conditions. *Mass Spectrom. Rev.* **2013**, *32*, 218−243.

(12) Zhu, Y.; Zang, Q.; Luo, Z.; He, J.; Zhang, R.; Abliz, Z. An Organ-Specific Metabolite Annotation Approach for Ambient Mass Spectrometry Imaging Reveals Spatial Metabolic Alterations of a Whole Mouse Body. *Anal. Chem.* **2022**, *94*, 7286−7294.

(13) Bjarnholt, N.; Li, B.; D'Alvise, J.; Janfelt, C. Mass Spectrometry Imaging of Plant Metabolites − Principles and Possibilities. *Nat. Prod. Rep.* **2014**, *31*, 818−837.

(14) Bhandari, D. R.; Wang, Q.; Friedt, W.; Spengler, B.; Gottwald, S.; Römpp, A. High Resolution Mass Spectrometry Imaging of Plant Tissues: Towards a Plant Metabolite Atlas. *Analyst* **2015**, *140*, 7696−7709.

(15) Eberlin, L. S.; Ferreira, C. R.; Dill, A. L.; Ifa, D. R.; Cooks, R. G. Desorption Electrospray Ionization Mass Spectrometry for Lipid Characterization and Biological Tissue Imaging. *Biochim. Biophys. Acta, Mol. Cell Biol. Lipids* **2011**, *1811*, 946−960.

(16) Hieta, J.-P.; Sipari, N.; Räikkönen, H.; Keinänen, M.; Kostiainen, R. Mass Spectrometry Imaging of Arabidopsis Thaliana Leaves at the Single-Cell Level by Infrared Laser Ablation Atmospheric Pressure Photoionization (LAAPPI). *J. Am. Soc. Mass Spectrom.* **2021**, *32*, 2895−2903.

(17) da Silva, M. A. O.; Arruda, M. A. Z. Laser Ablation (Imaging) for Mapping and Determining Se and S in Sunflower Leaves. *Metallomics* **2013**, *5*, 62−67.

(18) Shroff, R.; Vergara, F.; Muck, A.; Svatos, A.; Gershenzon, J. Nonuniform Distribution of Glucosinolates in *Arabidopsis Thaliana* Leaves Has Important Consequences for Plant Defense. *Proc. Natl. Acad. Sci. U.S.A.* **2008**, *105*, 6196−6201.

(19) Mullen, A. K.; Clench, M. R.; Crosland, S.; Sharples, K. R. Determination of Agrochemical Compounds in Soya Plants by Imaging Matrix-Assisted Laser Desorption/Ionisation Mass Spectrometry. *Rapid Commun. Mass Spectrom.* **2005**, *19*, 2507−2516.

(20) Lohse, M.; Haag, R.; Lippold, E.; Vetterlein, D.; Reemtsma, T.; Lechtenfeld, O. J. Direct Imaging of Plant Metabolites in the Rhizosphere Using Laser Desorption Ionization Ultra-High Resolution Mass Spectrometry. *Front. Plant Sci.* **2021**, *12*, No. 2733.

(21) Egoshi, S.; Dodo, K.; Sodeoka, M. Deuterium Raman Imaging for Lipid Analysis. *Curr. Opin. Chem. Biol.* **2022**, *70*, No. 102181.

(22) Xu, J.; Zhu, D.; Ibrahim, A. D.; Allen, C. C. R.; Gibson, C. M.; Fowler, P. W.; Song, Y.; Huang, W. E. Raman Deuterium Isotope Probing Reveals Microbial Metabolism at the Single-Cell Level. *Anal. Chem.* **2017**, *89*, 13305−13312.

(23) Wang, Y.; Xu, J.; Kong, L.; Liu, T.; Yi, L.; Wang, H.; Huang, W. E.; Zheng, C. Raman−Deuterium Isotope Probing to Study Metabolic Activities of Single Bacterial Cells in Human Intestinal Microbiota. *Microb. Biotechnol.* **2020**, *13*, 572−583.

(24) Yamakoshi, H.; Dodo, K.; Palonpon, A.; Ando, J.; Fujita, K.; Kawata, S.; Sodeoka, M. Alkyne-Tag Raman Imaging for Visualization of Mobile Small Molecules in Live Cells. *J. Am. Chem. Soc.* **2012**, *134*, 20681−20689.

(25) Bi, X.; Miao, K.; Wei, L. Alkyne-Tagged Raman Probes for Local Environmental Sensing by Hydrogen−Deuterium Exchange. *J. Am. Chem. Soc.* **2022**, *144*, 8504−8514.

(26) Dodo, K.; Sato, A.; Tamura, Y.; Egoshi, S.; Fujiwara, K.; Oonuma, K.; Nakao, S.; Terayama, N.; Sodeoka, M. Synthesis of Deuterated γ-Linolenic Acid and Application for Biological Studies: Metabolic Tuning and Raman Imaging. *Chem. Commun.* **2021**, *57*, 2180−2183.

(27) Matanfack, G. A.; Taubert, M.; Guo, S.; Bocklitz, T.; Küsel, K.; Rösch, P.; Popp, J. Monitoring Deuterium Uptake in Single Bacterial Cells via Two-Dimensional Raman Correlation Spectroscopy. *Anal. Chem.* **2021**, *93*, 7714−7723.

(28) Hosokawa, M.; Ando, M.; Mukai, S.; Osada, K.; Yoshino, T.; Hamaguchi, H. O.; Tanaka, T. In Vivo Live Cell Imaging for the Quantitative Monitoring of Lipids by Using Raman Microspectroscopy. *Anal. Chem.* **2014**, *86*, 8224−8230.

(29) Ozeki, Y.; Umemura, W.; Otsuka, Y.; Satoh, S.; Hashimoto, H.; Sumimura, K.; Nishizawa, N.; Fukui, K.; Itoh, K. High-Speed Molecular Spectral Imaging of Tissue with Stimulated Raman Scattering. *Nat. Photonics* **2012**, *6*, 845−851.

(30) Egawa, M.; Iwanaga, S.; Hosoi, J.; Goto, M.; Yamanishi, H.; Miyai, M.; Katagiri, C.; Tokunaga, K.; Asai, T.; Ozeki, Y. Label-Free Stimulated Raman Scattering Microscopy Visualizes Changes in Intracellular Morphology during Human Epidermal Keratinocyte Differentiation. *Sci. Rep.* **2019**, *9*, No. 12601.

(31) Shou, J.; Oda, R.; Hu, F.; Karasawa, K.; Nuriya, M.; Yasui, M.; Shiramizu, B.; Min, W.; Ozeki, Y. Super-Multiplex Imaging of Cellular Dynamics and Heterogeneity by Integrated Stimulated Raman and Fluorescence Microscopy. *iScience* **2021**, *24*, No. 102832.

(32) Delker, C.; Stenzel, I.; Hause, B.; Miersch, O.; Feussner, I.; Wasternack, C. Jasmonate Biosynthesis in *Arabidopsis Thaliana* - Enzymes, Products, Regulation. *Plant Biol.* **2006**, *8*, 297−306.

(33) Meï, C.; Michaud, M.; Cussac, M.; Albrieux, C.; Gros, V.; Maréchal, E.; Block, M. A.; Jouhet, J.; Rébeillé, F. Levels of Polyunsaturated Fatty Acids Correlate with Growth Rate in Plant Cell Cultures. *Sci. Rep.* **2015**, *5*, No. 15207.

(34) Gu, Y.; Zavaliev, R.; Dong, X. Membrane Trafficking in Plant Immunity. *Mol. Plant* **2017**, *10*, 1026−1034.

(35) Ferreira, D.; Figueiredo, J.; Laureano, G.; Machado, A.; Arrabaça, J. D.; Duarte, B.; Figueiredo, A.; Matos, A. R. Membrane Remodelling and Triacylglycerol Accumulation in Drought Stress Resistance: The Case Study of Soybean Phospholipases A. *Plant Physiol. Biochem.* **2021**, *169*, 9−21.

(36) Tasseva, G.; Richard, L.; Zachowski, A. Regulation of Phosphatidylcholine Biosynthesis under Salt Stress Involves Choline Kinases in *Arabidopsis Thaliana*. *FEBS Lett.* **2004**, *566*, 115−120.

(37) Wang, Y.; Zhang, X.; Huang, G.; Feng, F.; Liu, X.; Guo, R.; Gu, F.; Zhong, X.; Mei, X. Dynamic Changes in Membrane Lipid Composition of Leaves of Winter Wheat Seedlings in Response to PEG-Induced Water Stress. *BMC Plant Biol.* **2020**, *20*, No. 84.

(38) Lu, J.; Xu, Y.; Wang, J.; Singer, S. D.; Chen, G. The Role of Triacylglycerol in Plant Stress Response. *Plants* **2020**, *9*, No. 472.

(39) Shiva, S.; Samarakoon, T.; Lowe, K. A.; Roach, C.; Vu, H. S.; Colter, M.; Porras, H.; Hwang, C.; Roth, M. R.; Tamura, P.; Li, M.; Schrick, K.; Shah, J.; Wang, X.; Wang, H.; Welti, R. Leaf Lipid Alterations in Response to Heat Stress of Arabidopsis Thaliana. *Plants* **2020**, *9*, No. 845.

(40) He, M.; Ding, N.-Z. Plant Unsaturated Fatty Acids: Multiple Roles in Stress Response. *Front. Plant Sci.* **2020**, *11*, No. 562785.

(41) Higashi, Y.; Okazaki, Y.; Myouga, F.; Shinozaki, K.; Saito, K. Landscape of the Lipidome and Transcriptome under Heat Stress in *Arabidopsis Thaliana*. *Sci. Rep.* **2015**, *5*, No. 10533.

(42) Tannert, M.; Balcke, G. U.; Tissier, A.; Köck, M. At4g29530 Is a Phosphoethanolamine Phosphatase Homologous to PECP1 with a Role in Flowering Time Regulation. *Plant J.* **2021**, *107*, 1072−1083.

(43) Jao, C. Y.; Roth, M.; Welti, R.; Salic, A. Metabolic Labeling and Direct Imaging of Choline Phospholipids in Vivo. *Proc. Natl. Acad. Sci. U.S.A.* **2009**, *106*, 15332−15337.

(44) Zhang, J.; Liu, H.; Sun, J.; Li, B.; Zhu, Q.; Chen, S.; Zhang, H. Arabidopsis Fatty Acid Desaturase FAD2 Is Required for Salt Tolerance during Seed Germination and Early Seedling Growth. *PLoS One* **2012**, *7*, No. e30355.

(45) Hou, Q.; Ufer, G.; Bartels, D. Lipid Signalling in Plant Responses to Abiotic Stress. *Plant, Cell Environ.* **2016**, *39*, 1029−1048.

(46) McGlew, K.; Shaw, V.; Zhang, M.; Kim, R. J.; Yang, W.; Shorrosh, B.; Suh, M. C.; Ohlrogge, J. An Annotated Database of Arabidopsis Mutants of Acyl Lipid Metabolism. *Plant Cell Rep.* **2015**, *34*, 519−532.

(47) Du, H.; Huang, M.; Hu, J.; Li, J. Modification of the Fatty Acid Composition in Arabidopsis and Maize Seeds Using a Stearoyl-Acyl Carrier Protein Desaturase-1 (ZmSAD1) Gene. *BMC Plant Biol.* **2016**, *16*, No. 137.

(48) Yasuda, M.; Takeshita, N.; Shigeto, S. Deuterium-Labeled Raman Tracking of Glucose Accumulation and Protein Metabolic Dynamics in *Aspergillus Nidulans* Hyphal Tips. *Sci. Rep.* **2021**, *11*, No. 1279.

(49) Veerabagu, M.; Rinne, P. L. H.; Skaugen, M.; Paul, L. K.; van der Schoot, C. Lipid Body Dynamics in Shoot Meristems: Production, Enlargement, and Putative Organellar Interactions and Plasmodesmal Targeting. *Front. Plant Sci.* **2021**, *12*, No. 674031.

(50) Paul, L. K.; Rinne, P. L. H.; van der Schoot, C. Refurbishing the Plasmodesmal Chamber: A Role for Lipid Bodies? *Front. Plant Sci.* **2014**, *5*, No. 40.

(51) Verslues, P. E.; Agarwal, M.; Katiyar-Agarwal, S.; Zhu, J.; Zhu, J.-K. Methods and Concepts in Quantifying Resistance to Drought, Salt and Freezing, Abiotic Stresses That Affect Plant Water Status. *Plant J.* **2006**, *45*, 523−539.

(52) Sánchez-Martín, J.; Canales, F. J.; Tweed, J. K. S.; Lee, M. R. F.; Rubiales, D.; Gómez-Cadenas, A.; Arbona, V.; Mur, L. A. J.; Prats, E. Fatty Acid Profile Changes During Gradual Soil Water Depletion in Oats Suggests a Role for Jasmonates in Coping With Drought. *Front. Plant Sci.* **2018**, *9*, No. 1077.

(53) Zinta, G.; AbdElgawad, H.; Peshev, D.; Weedon, J. T.; Van den Ende, W.; Nijs, I.; Janssens, I. A.; Beemster, G. T. S.; Asard, H. Dynamics of Metabolic Responses to Periods of Combined Heat and Drought in *Arabidopsis Thaliana* under Ambient and Elevated Atmospheric CO2. *J. Exp. Bot.* **2018**, *69*, 2159−2170.

(54) Mishra, M. K.; Singh, G.; Tiwari, S.; Singh, R.; Kumari, N.; Misra, P. Characterization of Arabidopsis Sterol Glycosyltransferase TTG15/UGT80B1 Role during Freeze and Heat Stress. *Plant Signaling Behav.* **2015**, *10*, No. e1075682.

(55) Mueller, S. P.; Krause, D. M.; Mueller, M. J.; Fekete, A. Accumulation of Extra-Chloroplastic Triacylglycerols in Arabidopsis Seedlings during Heat Acclimation. *J. Exp. Bot.* **2015**, *66*, 4517−4526.

(56) Yaghmour, M. H.; Thiele, C.; Kuerschner, L. An Advanced Method for Propargylcholine Phospholipid Detection by Direct-Infusion MS. *J. Lipid Res.* **2021**, *62*, No. 100022.

(57) Yamakoshi, H.; Ohori, H.; Kudo, C.; Sato, A.; Kanoh, N.; Ishioka, C.; Shibata, H.; Iwabuchi, Y. Structure−Activity Relationship of C5-Curcuminoids and Synthesis of Their Molecular Probes Thereof. *Bioorg. Med. Chem.* **2010**, *18*, 1083−1092.

(58) Ozeki, Y.; Asai, T.; Shou, J.; Yoshimi, H. Multicolor Stimulated Raman Scattering Microscopy With Fast Wavelength-Tunable Yb Fiber Laser. *IEEE J. Sel. Top. Quantum Electron.* **2019**, *25*, 1−11.

(59) Jenkin, S.; Molina, I. Isolation and Compositional Analysis of Plant Cuticle Lipid Polyester Monomers. *J. Visualized Exp.* **2015**, No. 53386.

(60) Murcha, M. W.; Whelan, J. Isolation of Intact Mitochondria from the Model Plant Species *Arabidopsis Thaliana* and Oryza Sativa. *Methods Mol. Biol.* **2015**, *1305*, 1−12.

(61) Engelberth, J.; Schmelz, E. A.; Alborn, H. T.; Cardoza, Y. J.; Huang, J.; Tumlinson, J. H. Simultaneous Quantification of Jasmonic Acid and Salicylic Acid in Plants by Vapor-Phase Extraction and Gas Chromatography-Chemical Ionization-Mass Spectrometry. *Anal. Biochem.* **2003**, *312*, 242−250.

(62) Wang, Z.; Benning, C. *Arabidopsis Thaliana* Polar Glycerolipid Profiling by Thin Layer Chromatography (TLC) Coupled with Gas-Liquid Chromatography (GLC). *J. Visualized Exp.* **2011**, *49*, No. 2518.